Probing the accelerating Universe with radio weak lensing in the JVLA Sky Survey

M. L. Brown[1*], F. B. Abdalla[2], A. Amara[3], D. J. Bacon[4], R. A. Battye[1], M. R. Bell[5], R. J. Beswick[1], M. Birkinshaw[6], V. Böhm[5], S. Bridle[1], I. W. A. Browne[1], C. M. Casey[7], C. Demetroullas[1], T. Enßlin[5,8], P. G. Ferreira[9], S. T. Garrington[1], K. J. B. Grainge[1], M. E. Gray[10], C. A. Hales[11], I. Harrison[1], A. F. Heavens[12], C. Heymans[13], C.-L. Hung[14], N. J. Jackson[1], M. J. Jarvis[9], B. Joachimi[2], S. T. Kay[1], T. D. Kitching[15], J. P. Leahy[1], R. Maartens[16,4], L. Miller[9], T. W. B. Muxlow[1], S. T. Myers[17], R. C. Nichol[4], P. Patel[16,18], J. R. Pritchard[12], A. Raccanelli[19,20], A. Refregier[3], A. M. S. Richards[1], C. Riseley[21], M. G. Santos[16,22], A. M. M. Scaife[21], B. M. Schäfer[23], R. T. Schilizzi[1], I. Smail[24], J.-L. Starck[25], R. M. Szepietowski[1], A. N. Taylor[13], L. Whittaker[1], N. Wrigley[1], J. Zuntz[1]

(Affiliations can be found after the references)

We outline the prospects for performing pioneering radio weak gravitational lensing analyses using observations from a potential forthcoming JVLA Sky Survey program. A large-scale survey with the JVLA can offer interesting and unique opportunities for performing weak lensing studies in the radio band, a field which has until now been the preserve of optical telescopes. In particular, the JVLA has the capacity for large, deep radio surveys with relatively high angular resolution, which are the key characteristics required for a successful weak lensing study. We highlight the potential advantages and unique aspects of performing weak lensing in the radio band. In particular, the inclusion of continuum polarisation information can greatly reduce noise in weak lensing reconstructions and can also remove the effects of intrinsic galaxy alignments, the key astrophysical systematic effect that limits weak lensing at all wavelengths. We identify a VLASS "deep fields" program (total area ∼10–20 deg^2), to be conducted at L-band and with high-resolution (A-array configuration), as the optimal survey strategy from the point of view of weak lensing science. Such a survey will build on the unique strengths of the JVLA and will remain unsurpassed in terms of its combination of resolution and sensitivity until the advent of the Square Kilometre Array. We identify the best fields on the JVLA-accessible sky from the point of view of overlapping with existing deep optical and near infra-red data which will provide crucial redshift information and facilitate a host of additional compelling multi-wavelength science.

1 Introduction

Weak gravitational lensing is the effect whereby images of faint and distant background galaxies are coherently distorted due to deflection of their light by intervening large scale structures in the Universe. This "cosmic shear" effect is recognised as one of the key cosmological probes that will allow us to precisely probe the nature of dark energy with future surveys (Albrecht et al., 2006; Peacock et al., 2006). The current state-of-the-art in terms of weak lensing comes from optical surveys covering 154 deg^2, i.e. the recent CFHTLenS results (Heymans et al., 2012). Although

*Corresponding author: m.l.brown@manchester.ac.uk

the lensing-derived constraints on the evolution of structure are currently not strong enough to meaningfully constrain the properties of dark energy, ongoing and future ground-based surveys, e.g. the KiDS (de Jong et al., 2013), DES[1], HSC[2], LSST[3] and SKA[4] surveys, and ultimately satellite missions such as NASA's *WFIRST*[5] and ESA's *Euclid*[6] telescope (Laureijs et al., 2011), promise to revolutionise the field of weak lensing by allowing precision measurements of structure growth. In addition, lensing measurements can be used to test the nature of gravity in a complementary way to other cosmological probes (e.g. Simpson et al. 2013; Raccanelli et al. 2012).

The only detection of weak lensing in the radio band to date was made by Chang et al. (2004) using the VLA FIRST survey (Becker et al., 1995). Since then progress in radio weak lensing studies has lagged behind the optical because of the much smaller number density of galaxies typically seen in radio surveys as compared to the optical bands. This situation is beginning to change with the advent of a new generation of radio telescopes. Indeed a number of relatively large observational programs in the radio have weak lensing as one of their primary science drivers. In particular the SuperCLASS[7] survey on the UK's e-MERLIN telescope aims to detect the weak lensing signal in a supercluster of galaxies while the CHILES[8] continuum and HI surveys, currently being undertaken on the JVLA, will search for radio weak lensing effects in the COSMOS field. Large scale surveys with the LOFAR telescope and with the SKA pathfinder telescopes, MeerKAT and ASKAP will also offer interesting opportunities for radio weak lensing studies (mainly through lensing magnification effects) in the run-up to Phase-1 of the SKA for which construction is due to start in 2017.

This new generation of radio telescopes can offer unique and powerful added value to the field of weak lensing. Firstly, deep radio surveys will probe the lensing power spectrum at significantly higher redshift than most of the planned optical lensing surveys. The addition of radio can therefore offer a more powerful redshift "lever arm" with which to measure the effects of dark energy on the evolution of structure. Secondly, instrumental systematic effects are a serious concern for weak lensing studies for which a very accurate representation of the beam or point spread function (PSF) of the telescope is required. The highly stable and deterministic beam response of radio interferometers could therefore prove a major advantage for weak lensing science. Thirdly, the radio offers unique and novel opportunities to measure the effects of weak lensing that are not available to optical lensing surveys through polarization measurements, HI rotational velocity measurements and the direct measurement of galaxy shapes in the uv visibility plane.

The JVLA's unique combination of excellent sensitivity and relatively high angular resolution will remain unsurpassed until the advent of the SKA. These qualities also make the JVLA an excellent facility with which to spearhead the development of radio weak lensing. Here, we describe how the JVLA could play a major role in this rapidly developing field through consideration of radio weak lensing science during the survey design for a new generation of VLA Sky Surveys (VLASS).

2 Optimal survey configurations for the VLASS

Here we examine the optimal configurations for a VLASS conducted at frequencies 1.4 (L-band), 3.0 (S-band) and 4.8 GHz (C-band). Using Fisher analyses and simple mode-counting arguments,

[1] http://www.darkenergysurvey.org
[2] http://www.naoj.org/Projects/HSC/
[3] https://www.lsstcorp.org
[4] https://www.skatelescope.org
[5] http://wfirst.gsfc.nasa.gov
[6] http://sci.esa.int/euclid/
[7] http://www.e-merlin.ac.uk/legacy/projects/superclass.html
[8] http://www.mpia-hd.mpg.de/homes/kreckel/CHILES/index.html

one can predict the achievable errors on the cosmic shear power spectrum with a given survey design. For our purposes, by "survey design", we simply mean the survey area and depth (the latter assumed to be constant across the survey). The forecasted errors on a measurement of the 2D cosmic shear power spectrum in a band of $\Delta\ell$, centred on a multipole, ℓ are

$$\Delta C_\ell = \sqrt{\frac{2}{(2\ell+1)\Delta\ell f_{\rm sky}}}\left[C_\ell + \frac{\gamma_{\rm rms}^2}{2n_g}\right], \tag{1}$$

where $f_{\rm sky}$ is the fraction of sky observed, n_g is the number density of source galaxies and $\gamma_{\rm rms}$ is the total dispersion in the galaxy ellipticity estimates due to both measurement errors and the intrinsic dispersion in galaxy shapes. We assume both to be ~ 0.3 resulting in an effective shear estimator dispersion of $\gamma_{\rm rms} = 0.42$. This is consistent with the observed shapes of galaxies in both deep optical surveys (e.g. Miller et al. 2013) and in deep radio observations (Patel et al., 2010).

C_ℓ is the power spectrum which we calculate in the concordance ΛCDM cosmology as

$$C_\ell = \int_0^{\chi_h} \frac{W^2(\chi)}{\chi^2} P_\delta(\ell/\chi, \chi)\, d\chi \tag{2}$$

where χ_h is the comoving distance to the horizon. $W(\chi)$ is the lensing efficiency function, which for a lens at comoving distance, χ_d and redshift, z_d is

$$W(\chi_d) = \frac{3H_0^2\Omega_m}{2c^2}\chi_d(1+z_d)\int_{\chi_d}^{\chi_h} f(\chi_s)\frac{(\chi_s-\chi_d)}{\chi_s}\, d\chi_s. \tag{3}$$

Here, $f(\chi)$ is the distribution of sources in comoving distance, specified by the source redshift distribution, $f(\chi)d\chi = n(z)\, dz$. Note that, in this work, we have considered only the measurement of a single projected 2D power spectrum (C_ℓ). However, more generally, given distance information (e.g. from photometric redshift estimates), one can extract additional cosmological information on the evolution of structure in the Universe by measuring the lensing power spectrum in a series of tomographic redshift bins, $C_\ell(z)$.

To calculate error forecasts for different survey designs, we require the redshift distribution of sources as a function of flux density threshold. Throughout this work we adopt a detection threshold of $S_{\rm tot} > 10\sigma$ where σ is the projected RMS image noise. We have obtained an estimate of the radio-frequency $n(z)$ from the Square Kilometre Array Design Studies (SKADS) simulation (Wilman et al., 2008) for flux density thresholds between 1 and 100 μJy. Fig. 1 shows how the normalized 1.4 GHz $n(z)$ changes with the detection threshold for only the star-forming galaxies included in the SKADS simulation. For similar detection thresholds the redshift distributions for the S-band and C-band galaxy populations in the simulation are broadly similar.

The SKADS simulation also provides us with an estimate of the galaxy surface number density for a given detection threshold. These are plotted in the left panel of Fig. 2 for the three VLA frequency bands considered here. Note that we have re-normalized the galaxy densities such that $N(S_{1.4\,\rm GHz} > 54\,\mu{\rm Jy}) \approx 1.5$ arcmin^{-2} in order to match the number counts seen in the deep radio surveys of the VLA + MERLIN HDF-North field (Muxlow et al., 2005) and the VLA-COSMOS Large and Deep surveys (Schinnerer et al., 2010). Our adopted number density normalization is mid-way between those of the "gold" ($N(S_{1.4\,\rm GHz} > 54\,\mu{\rm Jy}) = 0.75$ arcmin^{-2}) and "silver" ($N(S_{1.4\,\rm GHz} > 54\,\mu{\rm Jy}) = 3.76$ arcmin^{-2}) galaxy samples constructed by Patel et al. (2010) who re-analysed the Muxlow et al. (2005) VLA + MERLIN data for the purposes of a radio weak lensing study.

A further crucial factor that can impact the performance of weak lensing studies is the angular resolution of the telescope in relation to the typical size of the galaxies for which one wishes to

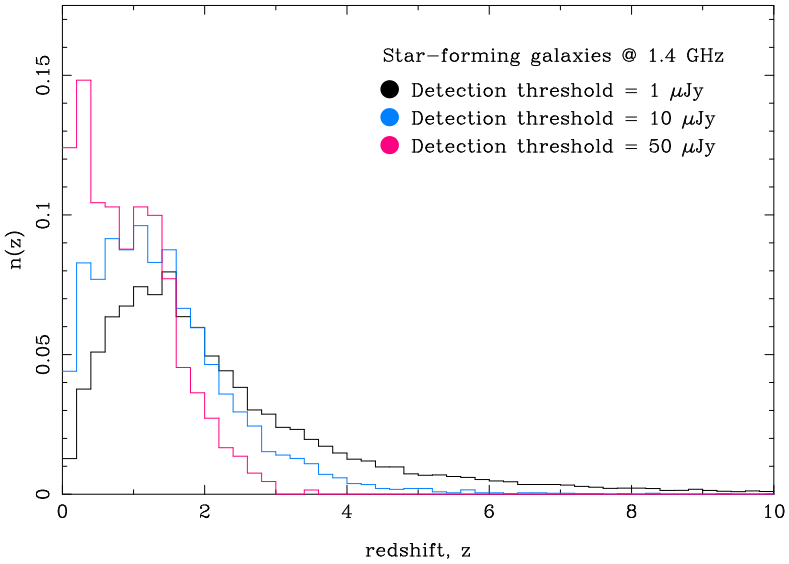

Figure 1: Redshift distribution of star-forming galaxies in the SKADS simulation for L-band detection thresholds of 1, 10 and 50 μJy. The distributions have median redshifts of $1.76, 1.25$ and 0.84 respectively and are normalized arbitrarily such that $\sum_z n(z) = 1$. For the same detection threshold, the S-band and C-band distributions are broadly similar to the L-band $n(z)$ although the total number of galaxies detected drops significantly (Fig. 2).

obtain accurate shape measurements. In the right panel of Fig. 2, we plot the distribution of galaxy sizes for two representative detection thresholds (10 and 20 μJy). Once again, these distributions have been derived from the SKADS simulation but they have been re-normalized to agree with observations. This re-normalization (which required a reduction in the sizes listed in the SKADS simulation by a factor of $\sim$3) was necessary to bring the mean galaxy size for the $S_{1.4\,\mathrm{GHz}} > 20$ μJy sample down to around 1 arcsec as found in a re-analysis of the Muxlow et al. (2005) MERLIN + VLA HDF-North observations (Wrigley et al. in prep.). For well-detected (e.g. $\gtrsim 10\sigma$) galaxies it is reasonable to assume that a good shape measurement is possible if the galaxy size is more than about 50% of the angular resolution of the telescope. Inspection of Fig. 2 then suggests a typical required angular resolution of $\sim$1 arcsec for a detection threshold of 10–20 μJy. Comparing to the resolution capabilities of the JVLA, the optimal array configuration would likely be A-array for L- and S-band observations (1.3 and 0.65 arcsec resolution respectively) while B-array would be appropriate for C-band observations (1.0 arcsec resolution). We note that for observations at S-band in A-array configuration, one would also need to consider how much of a typical galaxy's large scale emission is resolved out and the resulting potential impact on required survey times. This should not be a problem at L-band for which the A-array resolution is well-matched to typical galaxy sizes.

To arrive at the optimal survey strategy for detecting cosmic shear for a given amount of telescope time, we keep the quantity $\sqrt{\Omega}/S_{\mathrm{rms}}$ fixed where Ω is the survey area and S_{rms} is the RMS noise in flux density. This relation is normalized using the survey speed parameters required to achieve 100 μJy image noise RMS as listed in the VLASS capabilities document[9] made available alongside the call for VLASS White papers.

[9]see https://science.nrao.edu/science/surveys/vlass/capabilities

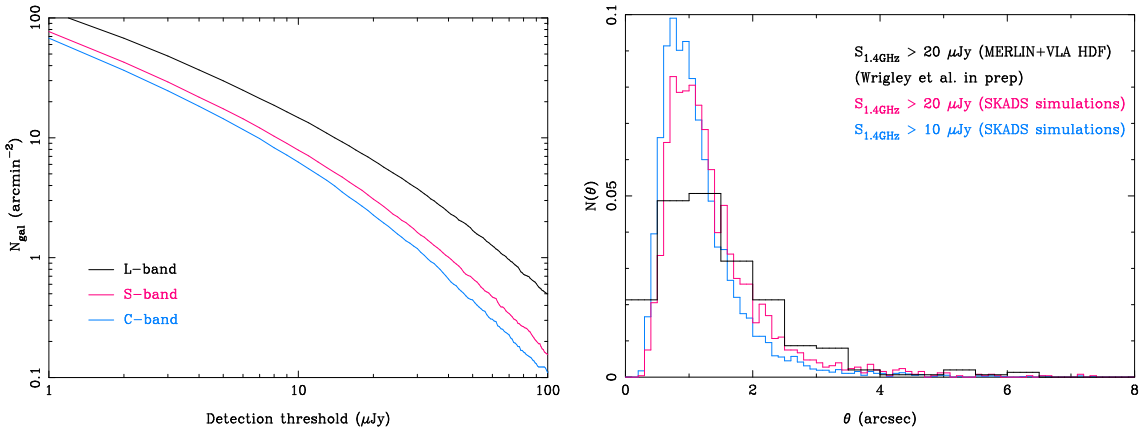

Figure 2: *Left panel:* The projected surface number density of galaxies as a function of the detection threshold for the JVLA's L-, S- and C-band frequency ranges. These projections have been obtained from the SKADS simulation, renormalized to match the observed counts of $N(S_{1.4\,\mathrm{GHz}} \gtrsim 50\,\mu\mathrm{Jy}) \approx 1.5$ arcmin^{-2} as measured in deep existing radio observations such as the VLA + MERLIN observations of the HDF-North (Muxlow et al., 2005) and the Large and Deep components of the VLA-COSMOS survey (Schinnerer et al., 2010). *Right panel:* Distribution of galaxy sizes for limiting flux densities of $S_{1.4\,\mathrm{GHz}} = 10$ and 20 μJy as measured from the SKADS simulation and re-normalized (reduced in size by a factor of ~ 3) to agree with the typical sizes of galaxies detected in the HDF-North. Also plotted are the actual measured sizes of galaxies as seen in a re-analysis of the MERLIN + VLA HDF data making use of size estimates for 339 galaxies at $S_{1.4\,\mathrm{GHz}} > 20\,\mu$Jy (Wrigley et al., in prep.). For most of the survey configurations we examine in this study, the majority of detected galaxies will be resolved by the VLASS and so will allow accurate shape measurements.

The signal-to-noise of the detection of cosmic shear is calculated as

$$S/N = \left(\sum_b P_b^2 / \sigma_b^2 \right)^{1/2} , \tag{4}$$

where the sum is over shear power spectrum bandpowers (P_b) and σ_b is the forecasted error on each bandpower (eq. 1). We calculate S/N as a function of the RMS noise flux density and survey area. Note that the minimum and maximum observable power spectrum multipoles are also determined by the survey configuration through the maximum survey dimension and the typical angular separation of nearest neighbour galaxies respectively. These effects are included in our power spectrum forecasts. Finally, the optimal survey configuration is chosen to be the one which maximizes the S/N. We have performed this survey optimization procedure for four cases of total observation time, $T_{\mathrm{obs}} = 1000, 3000, 5000$, and 10000 hours. The predicted constraints on the shear power spectrum for the optimal survey found in each case are shown in Fig. 3.

Table 1 lists the survey area and S/N values for the optimal survey for each T_{obs} and frequency band considered. We see that for the largest survey duration of $T_{\mathrm{obs}} = 10000$ hrs, we could expect to detect the cosmic shear signal at $> 3\sigma$ even if the survey were to be conducted at C-band (although one would have to spend all of that time integrating on only 2 square degrees of sky). At L-band the $T_{\mathrm{obs}} = 10000$ hours survey could lead to a $\sim 10\sigma$ detection which is approaching the sensitivity of the most sensitive optical lensing surveys conducted to date. Note that to achieve this

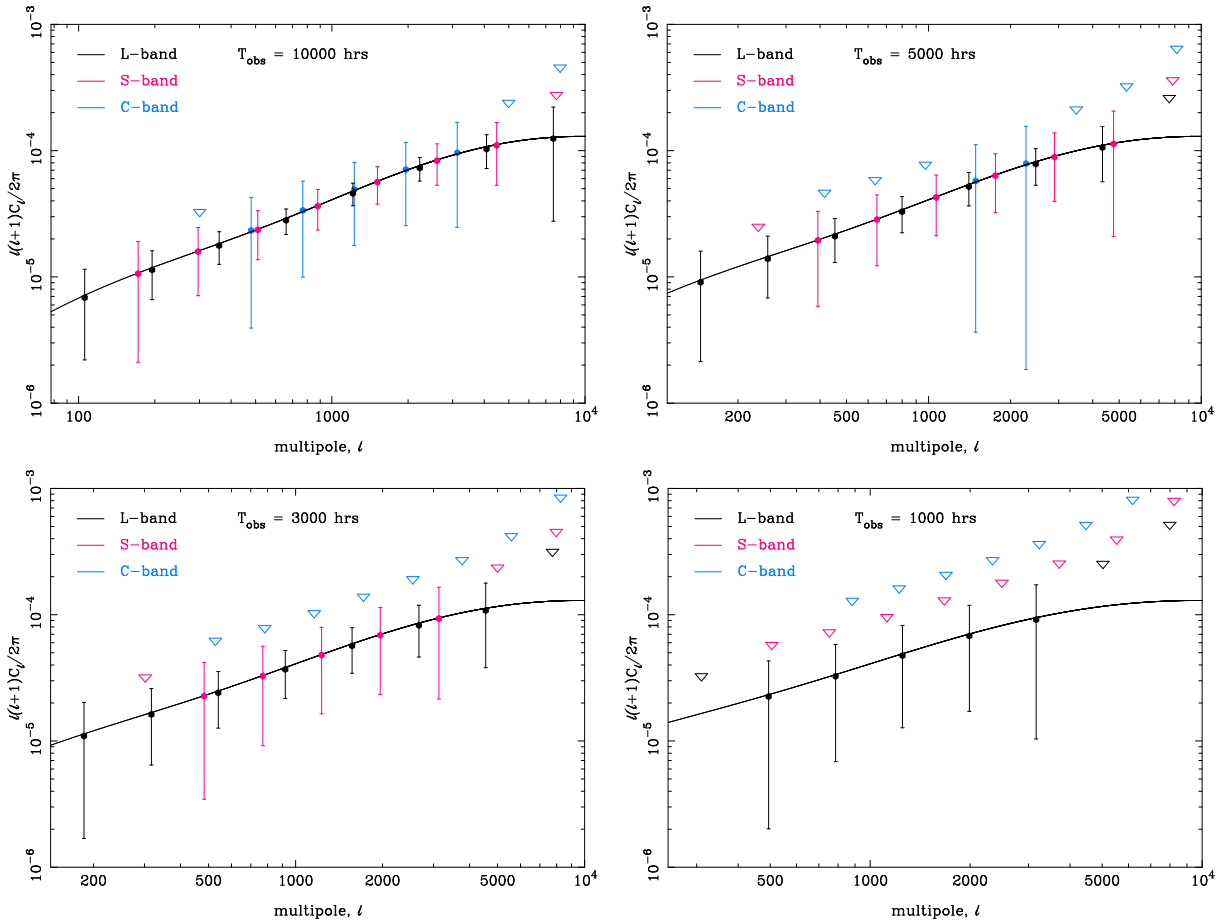

Figure 3: Forecasted constraints on the weak lensing power spectrum for the optimal L-, S- and C-band survey configurations for observing times of 10000 (*upper left*), 5000 (*upper right*), 3000 (*lower left*) and 1000 (*lower right*) hours. Open wedges indicate upper limits.

10σ detection, once again, one would need to concentrate on a relatively small field (~ 20 square degrees).

It is interesting to examine how the S/N of the detection depends on the adopted RMS image noise and survey size. These dependencies are demonstrated in Fig. 4 where we plot the S/N curves for each frequency band for the $T_{\rm obs} = 10000$ and $T_{\rm obs} = 3000$ hrs cases. The left hand panel of Fig. 4 shows S/N as a function of RMS noise. We see that the optimal image noise RMS level is insensitive to the survey time adopted, remaining at ~ 1 μJy for the L-band survey for both values of $T_{\rm obs}$. Similarly for the S- and C-band surveys, the preferred image RMS noise levels are ~ 0.6 μJy and ~ 0.5 μJy respectively independent of survey time. The corresponding preferred galaxy number density in all three cases is ~ 15 arcmin^{-2}. Note that these conclusions would change to some degree if we were to change the measure which we wish to optimize. For example, if we were to optimize on the survey's ability to constrain the very large scale power spectrum (for instance only multipoles $\ell < 100$), then a higher noise level would be preferred as the relative importance of the sample variance and noise variance terms in eq. (1) would have been altered.

The right hand panel of Fig. 4 shows the S/N as a function of survey area again for the $T_{\rm obs} = 10000$ and $T_{\rm obs} = 3000$ hrs cases. As expected, we see the preferred survey areas increasing

Table 1: Optimal survey areas and shear power spectrum detection significances for different observing times at L-band, S-band and C-band. The first column lists the assumed observation time in hours. The following six columns list the optimal survey area in square degrees (Ω) and the corresponding signal-to-noise of the weak lensing power spectrum detection ($C_\ell^{\rm lens}$ S/N) for the three frequency bands. The required depths (in terms of image RMS) are $\sim 1\,\mu$Jy, $0.6\,\mu$Jy and $0.5\,\mu$Jy for L-, S- and C-band respectively, independent of observation time.

$T_{\rm obs}$ (hrs)	Ω (deg^2) (L-band)	$C_\ell^{\rm lens}$ S/N (L-band)	Ω (deg^2) (S-band)	$C_\ell^{\rm lens}$ S/N (S-band)	Ω (deg^2) (C-band)	$C_\ell^{\rm lens}$ S/N (C-band)
1000	1.7	3.0	0.6	1.9	0.2	0.9
3000	5.0	5.4	1.8	3.4	0.5	1.8
5000	8.4	7.0	3.0	4.4	0.9	2.4
10000	16.8	9.9	6.0	6.3	1.8	3.5

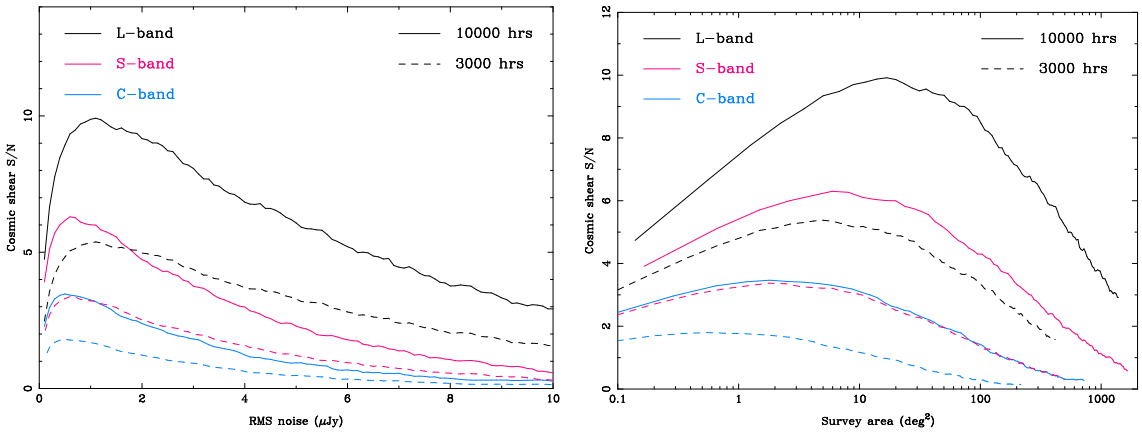

Figure 4: The signal-to-noise with which the shear power spectrum is detected for the 3000 and 10000 hours survey in each frequency band as a function of RMS noise (*left panel*) and survey area (*right panel*). The corresponding plots for the other survey times investigated look broadly similar with the optimal survey areas increasing with increasing observation time.

as we increase the observation time. Perhaps the most useful aspect of this plot is the ability to identify the range of survey areas over which the S/N remains approximately constant for a given survey duration. It is clear from the figure that the S/N curves become more peaked for longer and deeper surveys meaning that this range is smaller for larger survey programs. Nevertheless, even for the most powerful radio weak lensing survey (10000 hrs @ L-band), the S/N is relatively constant for survey areas between $\sim$ 10 and $\sim$ 100 square degrees. For ease of comparison, in Table 2, we report the S/N values for all of the survey configurations that we have investigated for the cases of $\Omega = 1, 10$ and 100 square degrees.

Table 2: Detection significances for the case of JVLA surveys covering 1, 10 and 100 deg^2 for different observing times, $T_{\rm obs}$ and for each of the L-, S-, and C-band channels.

	$C_\ell^{\rm lens}$ S/N $\Omega = 1$ deg^2	$C_\ell^{\rm lens}$ S/N $\Omega = 10$ deg^2	$C_\ell^{\rm lens}$ S/N $\Omega = 100$ deg^2
10000 hrs @ L-band	6.9	9.2	8.4
5000 hrs @ L-band	5.6	6.9	5.0
3000 hrs @ L-band	4.7	5.0	3.4
1000 hrs @ L-band	3.1	2.6	1.1
10000 hrs @ S-band	4.7	5.9	4.2
5000 hrs @ S-band	3.6	4.2	2.3
3000 hrs @ S-band	2.9	2.8	1.4
1000 hrs @ S-band	1.7	1.2	0.3
10000 hrs @ C-band	3.2	3.0	1.4
5000 hrs @ C-band	2.0	1.7	0.6
3000 hrs @ C-band	1.7	1.1	0.3
1000 hrs @ C-band	0.8	0.4	0.1

3 The unique value of weak lensing in the radio

One of the most compelling reasons for pursuing measurements of weak lensing in the radio band is the unique added value that radio lensing can offer above and beyond the traditional optical-based approaches. One unique advantage is the polarization information that is available in the radio and which can provide information on the intrinsic (unlensed) shapes of background galaxies. As described in Brown & Battye (2011a), the position angle of the integrated polarized emission from a background galaxy is unaffected by gravitational lensing. If the polarized emission (which is polarized synchrotron emission sourced by the galaxy's magnetic field) is also strongly correlated with the disk structure of the galaxy then measurements of the radio polarization position angle can be used as estimates of the galaxy's intrinsic (unlensed) position angle.

Such an approach could potentially have two key advantages over traditional weak lensing analyses. Firstly, the polarization technique can be used to effectively remove the primary astrophysical contaminant of weak lensing measurements – intrinsic galaxy alignments (see e.g. Heavens et al. 2000; Catelan et al. 2001; Hirata & Seljak 2004; Brown et al. 2002) – which are a severe worry for ongoing and future precision cosmology experiments based on weak lensing. Secondly, depending on the polarization properties of distant background disk galaxies, the polarization technique has the potential to reduce the effects of noise due to the intrinsic dispersion in galaxy shapes. Using the polarization technique, the forecasted errors on a measurement of the shear power spectrum becomes (Brown & Battye, 2011b)

$$\Delta C_\ell = \sqrt{\frac{2}{(2\ell+1)\Delta\ell f_{\rm sky}}}\left[C_\ell + \frac{16\alpha_{\rm rms}^2\gamma_{\rm rms}^2}{2n_{\rm pol}}\right], \tag{5}$$

where $\alpha_{\rm rms}$ is the scatter in the relationship between the observed polarization position angle and the intrinsic structural position angle of the galaxy and $n_{\rm pol} \approx f_{\rm pol} n_g$ is the number of galaxies

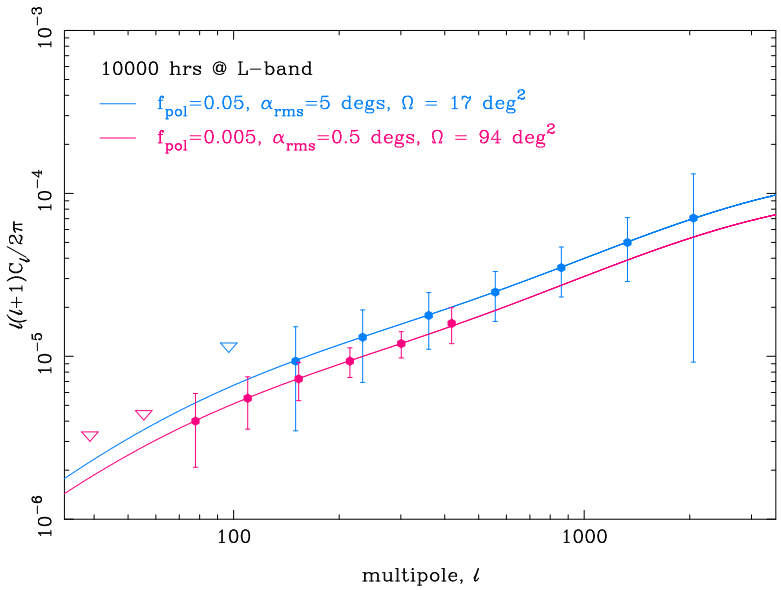

Figure 5: Forecasts of the constraints on the shear power spectrum obtainable with a 10000 hour L-band survey using the polarization technique described in the text. The observational parameters, $f_{\rm pol}$ and $\alpha_{\rm rms}$, appropriate for the faint μJy galaxy population are unknown at this time so we present forecasts for two possible cases. The forecasted constraints are restricted to the low-ℓ (linear) part of the power spectrum due to the assumed low surface number density of galaxies with measurable polarization.

for which one can obtain accurate polarization measurements. These parameters depend on the details of the polarization properties of background galaxies (e.g. the mean polarization fraction, $\Pi_{\rm pol}$) which are currently not well known. There are some existing measurements for a sample of local spiral galaxies (Stil et al., 2009) which suggest $\alpha_{\rm rms} < 15^\circ$ and $\Pi_{\rm pol} < 20\%$ although the sample is small.

In Fig. 5, we plot the forecasted constraints that could be achieved with a 10000 hr L-band survey for two representative cases: $\{\alpha_{\rm rms} = 5^\circ; f_{\rm pol} = 5\%\}$ and $\{\alpha_{\rm rms} = 0.5^\circ; f_{\rm pol} = 0.5\%\}$. Once again, in each case we plot the forecasts for the optimal survey area and depth which was identified as described in the previous section. It is clear from eq. (5) that the polarization technique becomes free of shape noise in the limit of $\alpha_{\rm rms} = 0$. A consequence of this behaviour is apparent in Fig. 5 – as $\alpha_{\rm rms}$ is reduced the shape noise contribution to the total error becomes sub-dominant and the optimization procedure pushes the survey area to larger areas. At the same time, a reduction in the mean polarization fraction, $\Pi_{\rm pol}$ will result in a low surface number density of galaxies which will limit the maximum multipole that can be probed with the polarization technique. Note also that it may be possible to select sub-samples of the total galaxy population to have particular polarization properties. For example, one could imagine that selecting only galaxies with high fractional polarization would yield a galaxy sub-sample with highly ordered magnetic fields which would consequently have a very tight correlation (low $\alpha_{\rm rms}$) between the polarization orientations and the intrinsic structural position angles of the galaxies. Of course, such a sub-sample would also have a very low surface number density of galaxies. The polarization technique may therefore be better suited to probing the shear power spectrum on large scales where high number densities are not required.

A second novel idea that is well suited to radio observations is to use rotational velocity mea-

surements to provide information about the intrinsic shapes of galaxies. The idea, first suggested by Blain (2002) and Morales (2006), is to measure the axis of rotation of a disk galaxy and to compare this to the orientation of the major axis of the galaxy disk image. In the absence of lensing, these two orientations should be perpendicular and measuring the departure from perpendicularity directly estimates the shear field at the galaxy's position. Such an analysis would require commensal HI line observations which could in principle be done at no extra cost in terms of telescope time. The rotation velocity technique shares many of the characteristics of the polarization approach described above – in the limit of perfectly well-behaved disk galaxies, it is also free of shape noise and it can also be used to remove the contaminating effect of intrinsic galaxy alignments. In practice, the degree to which the rotational velocity technique improves on standard methods will be dependent on observational parameters analogous to the ones for polarization discussed above. First, one would need to account for the fact that the HI line emission of galaxies is much fainter than the broad-band continuum emission and so the number of galaxies will be reduced (equivalent to the $n_{\rm pol}$ parameter discussed above); and secondly, for a population of real disk galaxies, there will again be some scatter in the relationship between the rotation axis and the major axis of the galaxy disk (equivalent to the $\alpha_{\rm rms}$ parameter in the polarization case). Recently, Huff et al. (2013) have proposed to extend this technique using the Tully-Fisher relation to calibrate the rotational velocity shear measurements and thus reduce the residual shape noise even further.

Both the polarization technique and the rotation velocity approach are currently being tested as part of the SuperCLASS and CHILES projects. They offer great promise for reducing the impact of shape noise and intrinsic alignments in radio weak lensing surveys. We note that the rotation velocity approach would not be feasible with a L-band A-array configuration survey due to the low surface brightness in HI. Nevertheless, the application of the polarization approach on the VLASS data is likely to be one of the most exciting aspects of the radio weak lensing analysis.

In addition to these new astrophysical probes, radio observations offer unique advantages for traditional lensing analyses by way of fitting for galaxy shapes directly from *uv*-visibility data (Chang & Refregier, 2002; Chang et al., 2004). Another unique aspect comes from the JVLA's wide bandwidth at L- and S-band which will allow the direct measurement of the frequency dependence of the beam. This is a potential major advantage over optical broad-band photometry where galaxy SEDs vary wildly while in the radio, galaxies typically exhibit smooth power-law type spectra.

4 Choice of observing fields and overlap with optical surveys

In Section 2 we have identified deep, high-resolution (A-array) L-band observations of relatively small sky areas ($\sim 10 - 100$ square degrees) as the optimal survey configuration from the point of view of maximising the sensitivity for cosmological weak lensing measurements. If the VLASS is to pursue such a strategy, the choice of field location is obviously a key consideration. Here, we identify the regions on the sky that are accessible to the JVLA and for which deep lensing quality optical and near infra-red (NIR) imaging already exists. The deep NIR data will be crucial as it will allow the estimation of photometric redshifts for galaxies in the range $1 < z < 2$ where a large fraction of the VLASS source galaxies are predicted to lie (see Fig. 1).

Fig. 6 shows the location of major northern and equatorial survey fields where deep optical and NIR imaging already exists. In addition to the CFHTLenS and KiDS surveys (which provide high-quality optical imaging data over large areas), also displayed are the location of five key deep field – the XMM-LSS, the Lockman Hole, the ELAIS N1 field, the SA22 field and the COSMOS field. These areas all include deep NIR observations (e.g. from the UKIDSS-DXS or VISTA VIDEO surveys) and hence would be ideal for supplying photometric redshift information to a VLASS deep

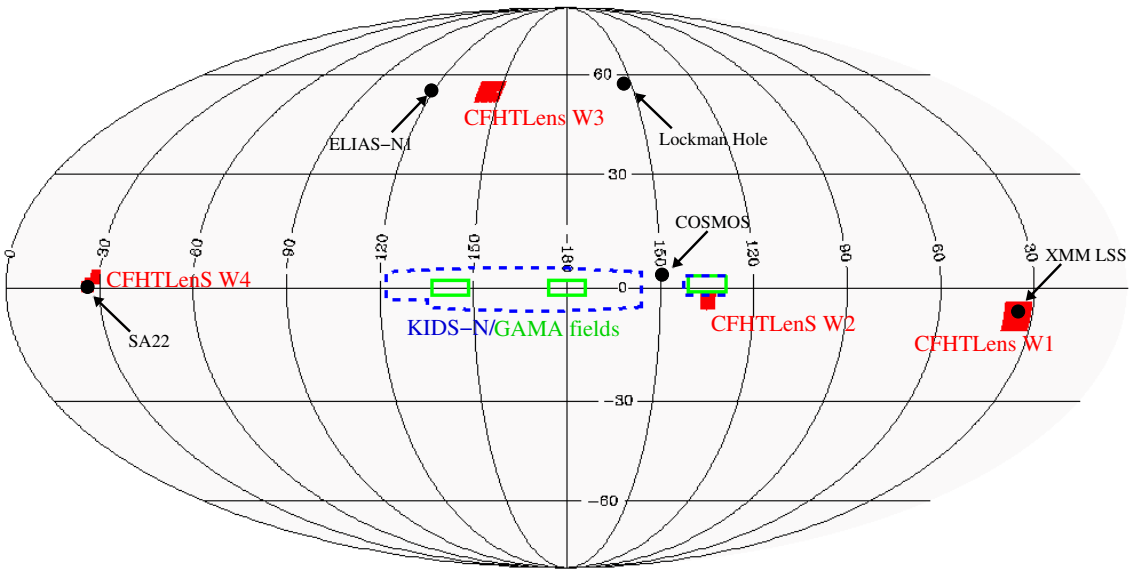

Figure 6: Field locations for some of the major deep optical and NIR surveys at Dec $\gtrsim 0°$. The projection is centred on (R. A. , Dec.) = (12 hrs, 0°). The four CFHTLenS fields are shown along with the large-area KiDS-N/GAMA field. The five fields containing deep NIR imaging crucial for obtaining redshift estimates for the proposed VLASS observations are indicated with filled black circles. Together they comprise ∼10–20 square degrees, ideally matched to the L-band VLASS survey area preferred in the lensing optimization analysis described in Section 2. These five well-studied regions would be excellent candidates for a program of targeted deep VLASS fields.

fields survey program. Each also offers a host of complementary observations at other wavebands.

In addition to providing redshifts, overlapping high quality optical imaging in these fields will provide a unique opportunity to test cross-correlation techniques that have been proposed with a view to mitigating instrumental systematics in weak lensing analyses (Jarvis & Jain, 2008; Patel et al., 2010). Although not the focus of this white paper, we note in passing that a deep A-array L-band survey targeting these well-studied fields would prove very interesting for a host of other extra-galactic science areas such as galaxy formation and evolution, star-formation studies out to high redshift, galaxy morphology studies and 3D clustering analyses of AGN and starburst galaxies.

5 Conclusions

We have explored the potential of large JVLA survey programs to provide a major step forward in the field of radio weak lensing. Of all of the SKA precursor and pathfinder telescopes, the JVLA is perhaps the instrument that is most suited to weak lensing work thanks to its unique combination of excellent sensitivity, relatively high angular resolution and relatively fast survey speeds. This white paper argues for a deep and high-resolution survey conducted over a relatively small survey area (a few 10s of square degrees) at L-band in A-array configuration. Such a survey will build on the JVLA's key strengths and will enable ground-breaking radio weak lensing science as well as many other compelling science goals in the areas of galaxy evolution, AGN clustering and understanding the physics and morphologies of star-forming and starburst galaxies to high redshift. Our key findings are:

- Depending on the duration of time devoted to a large VLASS program, a radio weak lensing

analysis of the VLASS could detect the effects of weak lensing by large scale structure with significances up to $\sim 10\sigma$. To achieve the upper limit of this range would require a 10000 hr deep radio survey over $\sim$ 10–20 deg^2 to be conducted at L-band in A-array configuration.

- Up to 7σ (5σ) detections could be achieved with a 5000 hr (3000 hr) L-band survey. The optimal survey area would be to focus on deep fields covering $\sim$10 square degrees.

- The weak lensing potential of the VLASS is reduced with increasing frequency. S-band could achieve a 4σ detection with a 5000 hr survey while a survey conducted at C-band would only exceed a 3σ detection with 10000 hrs of telescope time.

- The radio band offers unique advantages for performing weak lensing studies. Both polarization information and rotational velocity measurements from HI line surveys hold great promise for reducing the effects of shape noise and minimizing the contaminating effects of intrinsic alignments. The polarization technique can only be used in the radio.

- If the VLASS are to pursue a deep fields strategy, the choice of fields should be informed by the location of existing high-quality optical and NIR data. We have identified five fields covering $\sim$10–20 square degrees where this information already exists and which would be good candidates for a VLASS deep fields program.

We conclude with a demonstration of how a weak lensing analysis of a VLASS deep fields program could significantly enhance the current state-of-the-art in terms of optical weak lensing measurements. Fig. 7 shows the forecasted constraints from the proposed $\sim$ 17 deg^2 10000 hr L-band survey with the corresponding forecasts for the current state-of-the-art survey (CFHTLenS) as well as the forecasts for two representative ongoing optical surveys, the KiDS and DES surveys. The latter two surveys, and the HSC survey, are to be conducted over the next 5 years, potentially on a similar timescale to a large VLASS program. We immediately see that the VLASS survey probes a redshift range that is completely complementary to the shallower redshifts of the optical surveys. The addition of the high redshift information from the VLASS would therefore greatly enhance studies of the growth of structure through lensing by adding additional high-redshift bins to a tomographic cosmic shear analysis. This would in turn result in improved constraints on dark energy parameters. Beyond this, novel radio-based approaches to weak lensing through the use of polarization and rotational velocity measurements may well yield the best route forward for dealing with the problem of intrinsic galaxy alignments, the most troublesome obstacle for future precision cosmology experiments based on weak lensing. Designing the forthcoming VLASS to accommodate the weak lensing science exploitation advocated in this paper will provide an ideal dataset on which to demonstrate and refine these novel techniques.

References

Albrecht A., Bernstein G., Cahn R., Freedman W. L., Hewitt J., Hu W., Huth J., Kamionkowski M., Kolb E. W., Knox L., Mather J. C., Staggs S., Suntzeff N. B., 2006, ArXiv Astrophysics e-prints

Becker R. H., White R. L., Helfand D. J., 1995, ApJ, 450, 559

Blain A. W., 2002, ApJL, 570, L51

Brown M. L., Battye R. A., 2011a, MNRAS, 410, 2057

—, 2011b, ApJL, 735, L23

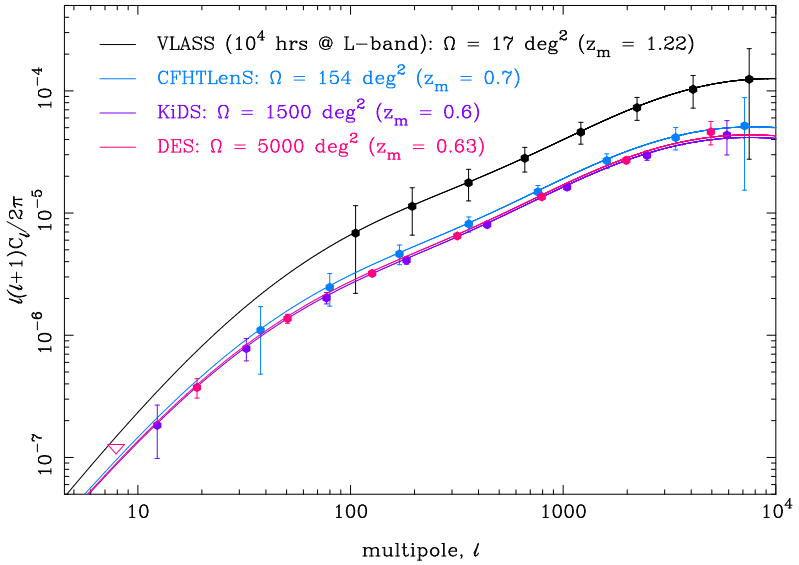

Figure 7: Performance of the optimal 17 deg^2 10000-hr L-band survey compared to the precision of current state-of-the art optical weak lensing survey (CFHTLenS) and two of the major ongoing weak lensing surveys (KiDS and DES). The KiDS, DES and HSC surveys will be conducted over the next 5 years, potentially on a similar timescale to a major VLASS. Note how the VLASS probes a much higher redshift range than the optical lensing surveys. The proposed VLASS would thus provide additional cosmological information on the evolution of structure at high-z beyond the reach of the optical-based lensing surveys. The forecasted detection significances of the constraints shown are $\sim 10\sigma$ (VLASS), 15σ (CFHTLenS), 30σ (KiDS) and 43σ (DES).

Brown M. L., Taylor A. N., Hambly N. C., Dye S., 2002, MNRAS, 333, 501

Catelan P., Kamionkowski M., Blandford R. D., 2001, MNRAS, 320, L7

Chang T., Refregier A., Helfand D. J., 2004, ApJ, 617, 794

Chang T.-C., Refregier A., 2002, ApJ, 570, 447

de Jong J. T. A., Verdoes Kleijn G. A., Kuijken K. H., Valentijn E. A., 2013, Exp. Astronomy, 35, 25

Heavens A., Refregier A., Heymans C., 2000, MNRAS, 319, 649

Heymans C., Van Waerbeke L., Miller L., Erben T., Hildebrandt H., Hoekstra H., Kitching T. D., Mellier Y., Simon P., Bonnett C., Coupon J., Fu L., Harnois Déraps J., Hudson M. J., Kilbinger M., Kuijken K., Rowe B., Schrabback T., Semboloni E., van Uitert E., Vafaei S., Velander M., 2012, MNRAS, 427, 146

Hirata C. M., Seljak U., 2004, Phys. Rev. D, 70, 063526

Huff E. M., Krause E., Eifler T., George M. R., Schlegel D., 2013, ArXiv e-prints

Jarvis M., Jain B., 2008, JCAP, 1, 3

Laureijs R., Amiaux J., Arduini S., Augueres J. ., Brinchmann J., Cole R., Cropper M., Dabin C., Duvet L., Ealet A., et al., 2011, ArXiv e-prints

Miller L., Heymans C., Kitching T. D., van Waerbeke L., Erben T., Hildebrandt H., Hoekstra H., Mellier Y., Rowe B. T. P., Coupon J., Dietrich J. P., Fu L., Harnois-Déraps J., Hudson M. J., Kilbinger M., Kuijken K., Schrabback T., Semboloni E., Vafaei S., Velander M., 2013, MNRAS, 429, 2858

Morales M. F., 2006, ApJL, 650, L21

Muxlow T. W. B., Richards A. M. S., Garrington S. T., Wilkinson P. N., Anderson B., Richards E. A., Axon D. J., Fomalont E. B., Kellermann K. I., Partridge R. B., Windhorst R. A., 2005, MNRAS, 358, 1159

Patel P., Bacon D. J., Beswick R. J., Muxlow T. W. B., Hoyle B., 2010, MNRAS, 401, 2572

Peacock J. A., Schneider P., Efstathiou G., Ellis J. R., Leibundgut B., Lilly S. J., Mellier Y., 2006, ESA-ESO Working Group on "Fundamental Cosmology". Tech. rep.

Raccanelli A., Zhao G.-B., Bacon D. J., Jarvis M. J., Percival W. J., Norris R. P., Röttgering H., Abdalla F. B., Cress C. M., Kubwimana J.-C., Lindsay S., Nichol R. C., Santos M. G., Schwarz D. J., 2012, MNRAS, 424, 801

Schinnerer E., Sargent M. T., Bondi M., Smolčić V., Datta A., Carilli C. L., Bertoldi F., Blain A., Ciliegi P., Koekemoer A., Scoville N. Z., 2010, ApJS, 188, 384

Simpson F., Heymans C., Parkinson D., Blake C., Kilbinger M., Benjamin J., Erben T., Hildebrandt H., Hoekstra H., Kitching T. D., Mellier Y., Miller L., Van Waerbeke L., Coupon J., Fu L., Harnois-Déraps J., Hudson M. J., Kuijken K., Rowe B., Schrabback T., Semboloni E., Vafaei S., Velander M., 2013, MNRAS, 429, 2249

Stil J. M., Krause M., Beck R., Taylor A. R., 2009, ApJ, 693, 1392

Wilman R. J., Miller L., Jarvis M. J., Mauch T., Levrier F., Abdalla F. B., Rawlings S., Klöckner H., Obreschkow D., Olteanu D., Young S., 2008, MNRAS, 388, 1335

---

[1]Jodrell Bank Centre for Astrophysics, University of Manchester, Oxford Road, Manchester M13 9PL, UK
[2]Department of Physics and Astronomy, University College London, Gower Street, London WC1E 6BT, UK
[3]Institute for Astronomy, ETH Zurich, Wolfgang-Pauli-Strasse 27, CH-8093 Zurich, Switzerland
[4]Institute for Cosmology & Gravitation, University of Portsmouth, Portsmouth, PO1 3FX, UK
[5]Max-Planck-Institut für Astrophysik, Karl-Schwarzschildstr. 1, 85748 Garching, Germany
[6]HH Wills Physics Laboratory, University of Bristol, Tyndall Avenue, Bristol BS8 1TL, UK
[7]Department of Physics & Astronomy, University of California, Irvine, CA 92697, USA
[8]Ludwig-Maximilians-Universität München, Geschwister-Scholl-Platz 1, 80539 Munich, Germany
[9]Astrophysics, University of Oxford, Denys Wilkinson Building, Keble Road, Oxford, OX1 3RH, UK
[10]School of Physics & Astronomy, University of Nottingham, University Park, Nottingham NG9 2RD, UK
[11]Janksy Fellow; National Radio Astronomy Observatory, Socorro, NM, 87801, USA
[12]Imperial Centre for Inference & Cosmology, Imperial College, Blackett Lab., London, SW7 2AZ, UK
[13]Institute for Astronomy, University of Edinburgh, Blackford Hill, Edinburgh EH9 3HJ, UK
[14]Institute for Astronomy, University of Hawaii, 2680 Woodlawn Drive, Honolulu, HI 96822, USA
[15]Mullard Space Science Laboratory, UCL, Holmbury St Mary, Dorking, Surrey RH5 6NT, UK
[16]Department of Physics, University of the Western Cape, Bellville 7535, South Africa
[17]National Radio Astronomy Observatory, Socorro, NM, 87801, USA
[18]Astrophysics, Cosmology Gravity Centre, University of Cape Town, Cape Town, 7701, South Africa
[19]Jet Propulsion Laboratory, California Institute of Technology, Pasadena CA 91109, USA
[20]California Institute of Technology, Pasadena CA 91125, USA
[21]School of Physics & Astronomy, University of Southampton, Highfield, Southampton, SO17 1BJ, UK
[22]CENTRA, IST, Universidade Tecnica de Lisboa, Av. Rovisco Pais 1, 1049-001 Lisboa, Portugal
[23]Universität Heidelberg, Monchhofstraße 12, 69120 Heidelberg, Germany
[24]Insititute for Computational Cosmology, Durham University, South Road, Durham DH1 3LE, UK
[25]CEA Saclay, IRFU, Service d'Astrophysique, 91191 Gif-Sur-Yvette CEDEX, France